AGU
ADVANCING EARTH AND SPACE SCIENCES

Geophysical Research Letters®

I. Schalko and M. Ponce contributed equally to this work.

Key Points:

- Deliberate wood placement can promote declogging adjacent to and downstream of logs
- Declogging was correlated with elevated turbulence downstream of logs and elevated velocity adjacent to logs
- Emergent logs declogged a greater surface area than submerged logs

Supporting Information:

Supporting Information may be found in the online version of this article.

Correspondence to:

I. Schalko,
isabella.schalko@wsl.ch

Flow and Turbulence Due To Wood Contribute to Declogging of Gravel Bed

I. Schalko[1,2,3] , **M. Ponce[4]** , **S. Lassar[2]**, **S. Schwindt[4]** , **S. Haun[4]** , and **H. Nepf[2]**

[1]Department of Mechanical and Process Engineering, Institute of Fluid Dynamics, ETH Zurich, Zurich, Switzerland, [2]Department of Civil and Environmental Engineering, Massachusetts Institute of Technology, Cambridge, MA, USA, [3]Swiss Federal Institute for Forest, Snow and Landscape Research WSL, Birmensdorf, Switzerland, [4]Institute for Modelling Hydraulic and Environmental Systems, University of Stuttgart, Stuttgart, Germany

Abstract The placement of wood in rivers is a common restoration method used to locally affect hydraulic and morphologic conditions to create habitat. Laboratory experiments demonstrated that wood placements can also promote surface declogging, that is, removal of fine sediment from a gravel bed, thereby restoring spawning grounds for fish. Logs of different size and submergence level were placed on a gravel bed clogged with fines. Surface declogging was observed in regions of elevated turbulence in the log wake and elevated velocity adjacent to the log. A criteria for declogging was identified based on a modified non-dimensional Shields parameter combining mean and turbulent velocity at the bed. The footprint of declogged bed scaled with log dimensions. Emergent logs produced a larger declogging footprint compared to submerged logs of the same length, due to their stronger influence on the flow field. Logs were also shown to prevent clogging over similar areas.

Plain Language Summary Placing wood in rivers is a common way of improving river health and creating regions for fish and small aquatic animals to live. This method involves the placement of individual wood pieces (logs) at the side or in the center of a river. In this study, we explored how the positioning of logs could be used to remove fine sediments from gravel beds by changing the way water flows. This is important because excessive deposition of fine sediments in the bed, defined as riverbed clogging, can make the channel bed too compact. This makes it harder for fish to find good spots to lay their eggs. Using laboratory experiments, we observed that the logs generated regions with strong water turbulence (swirling) and faster flowing water in their surroundings, both of which removed fines from the gravel bed surface. We identified specific conditions necessary for effective removal of fines, which were related to both the turbulence and water velocity. The size of the cleaned area on the gravel bed was proportional to the size of the log.

1. Introduction

Many rivers worldwide are modified and ecologically impaired due to human intervention such as channelization, land use practice, or dams (Kondolf et al., 2014; Wohl et al., 2015). One example is increased infiltration of fine sediments into the grain structure of gravel-dominated rivers (Cunningham et al., 1987; Einstein, 1968). This process is called riverbed clogging or colmation, while the reverse process is called declogging (Figure 9 in Schwindt et al., 2023). Clogging reduces the pore space both at the surface (surface clogging) and deeper in the substrate (subsurface clogging, Dubuis & De Cesare, 2023). This leads to a decrease in permeability and hydraulic conductivity of the riverbed, which in turn alters the hyporheic exchange between the channel and subsurface (Kemp et al., 2011; Owens et al., 2005; Schälchli, 1992). Clogging can degrade the habitat for macroinvertebrates (Jones et al., 2012) and fish (Lisle, 1989), for example, by decreasing the potential for making spawning redds (Sear, 1993; Wood & Armitage, 1997; Wooster et al., 2008).

To counteract river degradation, numerous restoration measures have been implemented. A common example is the placement of wood (Gurnell et al., 2002; Wohl et al., 2019), which creates heterogeneous flow conditions and morphological structures (Gippel, 1995; Keller & Swanson, 1979; Roni et al., 2015) and affects sediment dynamics (Faustini & Jones, 2003; Wohl & Scott, 2017). Wood placements can be used as a tool to initiate sediment motion in the area surrounding wood (Schalko & Nepf, 2020), to vary flow velocity and turbulence in the downstream wake (Müller et al., 2022; Schalko et al., 2021; Schnauder et al., 2022), and potentially to promote declogging (Schwindt et al., 2023). By generating local variation in hydraulic head, wood can also increase

Visualization: I. Schalko, M. Ponce
Writing – original draft: I. Schalko,
M. Ponce
Writing – review & editing: I. Schalko,
M. Ponce, S. Schwindt, S. Haun, H. Nepf

hyporheic exchange (Ader et al., 2021; Doughty et al., 2020; Sawyer et al., 2011; Wilhelmsen et al., 2021). Variation in wood placement geometry can be used to create different degrees of flow modification. For example, emergent logs placed at the channel center result in higher turbulent kinetic energy (TKE) in the wake and higher velocity adjacent to logs compared to submerged logs (Schalko et al., 2021).

In this study, we hypothesized that wood placements could promote surface declogging or reduce surface clogging by modifying local flow conditions. Specifically, the generation of elevated turbulence in the log wake and elevated flow velocity adjacent to the log may reduce or inhibit clogging. Flume experiments were conducted for different wood placements to investigate this hypothesis.

2. Materials and Methods

### 2.1. Test Setup and Procedure

Laboratory experiments were conducted in a 12.2 m long recirculating channel. The test section with a mobile bed was 6.0 m long and 0.6 m wide. A ramp of cobbles with a diameter of ≈ 0.05 m was used at the up- and downstream boundaries of the test section to provide a smooth transition from the fixed to the mobile bed (Figure 1a). The mobile bed was $h_b = 0.08$ m thick, $L_b = 6.0$ m long, and consisted of uniform bed material to avoid armoring effects. The bed material had a density of 2,650 kg/m³ (Quartz) and a mean grain diameter $d_m = 2.2$ mm. The model fine sediment was walnut grit, with a density of 1,300 kg/m³, a mean diameter $d_{m,w} = 0.26$ mm, and a settling velocity $w_s = 0.009$ m/s based on Equations 1a–1c in Supporting Information S1. We selected the model fine material to match the ratio of w_s to the shear velocity u_* observed for real fines in the field. For our tests, w_s/u_* was 0.48 ± 0.03 (mean $\pm$ standard error), which is comparable to ratios estimated for gravel bed rivers (Text S1 in Supporting Information S1).

The channel-averaged velocity was $U = Q/(B\,h)$, with Q = discharge, B = channel width, and h = water depth, measured at the beginning of the test section, corresponding to undisturbed conditions (Table 1). Longitudinal profiles of streamwise (u) and cross-stream (v) velocity were taken with a Nortek Vectrino at the log center, log edges, and center of the open-flow section without logs. At each point, velocity was sampled at 200 Hz for 120 s, which was sufficient to reach convergence. The velocity records were despiked and filtered according to Goring and Nikora (2002). Each velocity record was decomposed into the time-mean (denoted by overbar) and fluctuating (denoted by a single prime) components. Because the vertical velocity was not available, TKE, denoted as k_t, was defined using u and v

$$k_t = 0.5\left(\overline{u'^2} + \overline{v'^2}\right) \tag{1}$$

Six total tests where run with logs with varying properties, arranged in different orientations and combinations, and with different initial conditions. Similar to previous studies (Schalko et al., 2021), PVC pipes were used as model logs with diameters $d = 0.057$ m (narrow) and 0.114 m (wide), and lengths $L = 0.20$ m (short), 0.30 m (medium), and 0.40 m (long). Log orientation included side (similar to groynes) and center of the channel, submerged and emergent, and scenarios including one, two, or more than two logs in the channel at a time (Figure 1; Table 1). Each test focused on an individual log (marked in bold in Figure 1). Two initial conditions were tested: declogging tests (denoted with a "D") in which the channel was already clogged when logs were added, and clogging inhibition (denoted with a "C") in which the gravel was clean when logs were added. Test D1 focused on a submerged log placed at the side (Log 1: medium length with wide diameter). Tests D2 and D4 studied submerged center logs (wide (Log 1) versus narrow (Log 3) diameter), and tests D3 and D5 investigated emergent center logs (medium (Log 1) versus short (Log 2) logs). Test C1 considered multiple logs (Figure 1). The declogging tests (Tests D1-D5 in Table 1) examined how log placements could promote declogging, and the gravel bed was clogged prior to log placement. First, 5.2 kg of walnut grit was mixed with water, and the slurry was added to the upstream section of the flume. The water was stirred by hand to keep the walnut grit in suspension until fines were deposited evenly along the entire test section. Without hand-stirring, we observed no resuspension, that is, the current alone over a bare bed produced no resuspension or declogging. Then, the channel was carefully drained to not disturb the channel bed, and top view images were taken to record the initial bed condition. Next, the logs were placed in the flume, water was carefully reintroduced, and the discharge was set and maintained for 5 hr. Finally, the channel was drained and top view images of the final bed condition were taken.

Sediment cores were used to infer the depth of influence attributed to the surface declogging. To avoid too much disruption to the bed, this was only done for two tests (D4 and D5). The procedure is described in Text S2 in
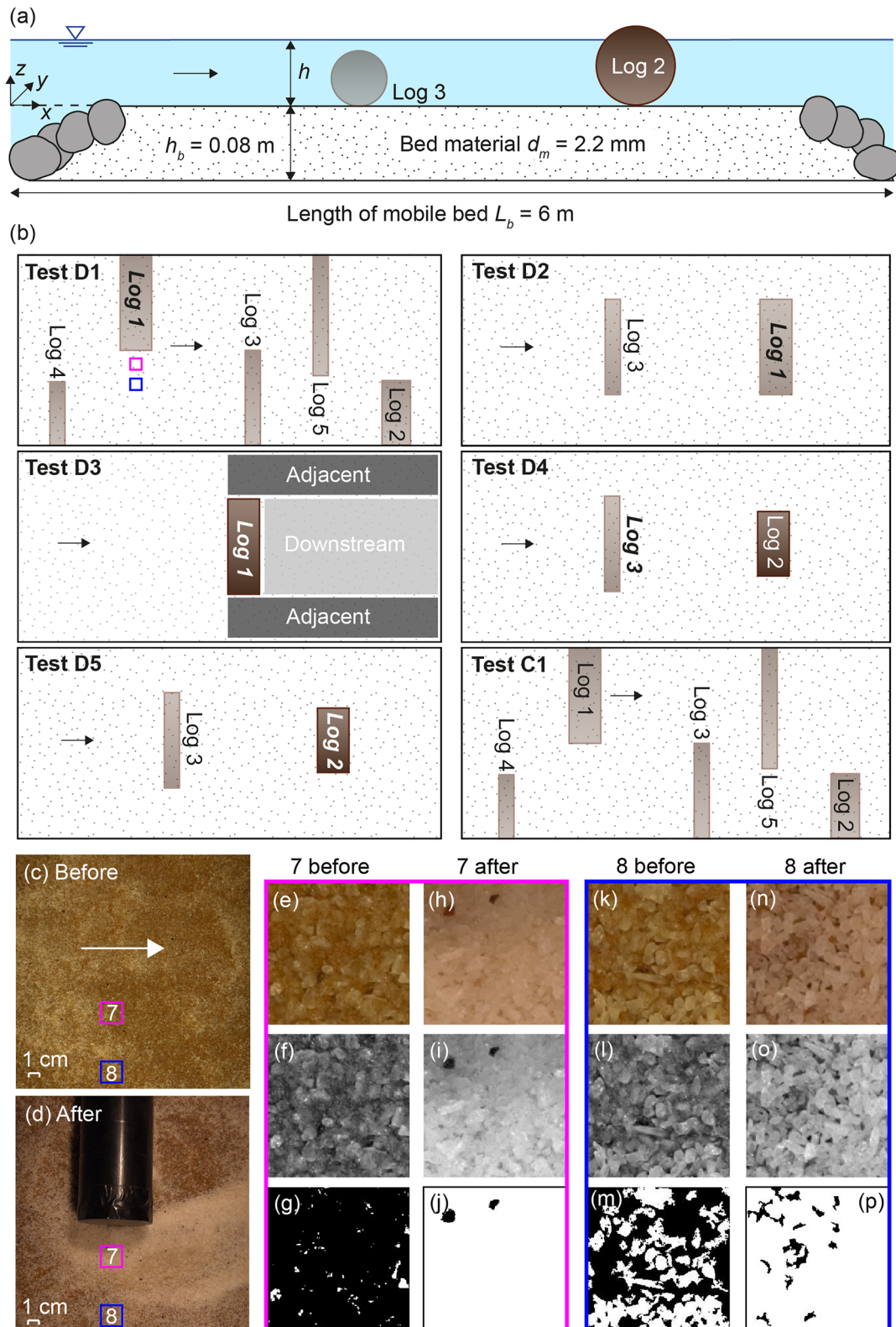
Figure 1. (a) Side view of test D4 and (b) top view of tests D1-D5, C1. Logs labeled in bold italic were the focus of the specific run. Emergent logs shown in dark brown and submerged in light brown. The downstream and adjacent areas are indicated for test D3. (c)–(p) Example of image analysis for two regions of interest (ROI): 7 (pink border) and 8 (blue border) (indicated in (b)). Top view images (c) before and (d) after test D1 next to Log 1. Original images in (e), (h), (k), (n), grayscale images in (f), (i), (l), (o), and final images with black areas indicating the following percent clogged area (g) 70.8%, (j) 1.0%, (m) 64.9%, (p) 18.5%.

Table 1
Test Program With Setups Shown in Figure 1

Test	Log number and position	Flow depth	Froude number	Discharge	Log diameter	Log length	Sub-mergence level	Standard deviation of $A_{c,pre}$	Mean fractional clogged area (post)	Mean degree of declogging
#	[-]	h [m]	F [-]	Q [l/s]	d [m]	L [m]	h/d [-]	$\sigma_{Ac,pre}$ [%]	$\overline{A_{c,post}}$ [%]	$\overline{\Delta\xi}$ [%]
D1	Log 1, side, submerged	0.13	0.19	16.7	0.11	0.30	1.14	17.5	35 ± 8	81 ± 8
D2	Log 1, center, submerged	0.14	0.17	16.7	0.11	0.30	1.23	7.1	33 ± 8	66 ± 7
D3	Log 1, center, emergent	0.06	0.33	8.0	0.11	0.30	0.53	8.3	22 ± 6	73 ± 6
D4	Log 3, center, submerged	0.08	0.21	8.9	0.06	0.30	1.40	6.2	57 ± 5	32 ± 5
D5	Log 2, center, emergent	0.08	0.21	8.9	0.11	0.20	0.70	11.6	27 ± 7	71 ± 5
C1	Multiple logs, side	0.12	0.22	17.2	0.06–0.11	0.20–0.40	2.10–1.05	–	–	–
	–	5%	5%	5%	1%	1%	5%	–	see SE per test	

Note. Standard deviation of fractional clogged area before test is $\sigma_{Ac,pre}$ and mean fractional clogged area after test is $\overline{A_{c,post}}$. Average percentage uncertainties are indicated in the last row for each variable. Standard error (SE) included in mean $\overline{A_{c,post}}$ and $\overline{\Delta\xi}$.

Supporting Information S1. At test end, clear acrylic pipes (inside diameter of 3 cm) were inserted into the gravel bed to extract 4 cm long cores. Sideview images of the cores were analyzed to estimate the depth of surface declogging, h_{dc}. Twelve cores were collected in test D4, and 14 in test D5. For an emergent log $h_{dc,m} = 6.6 \pm 0.8$ mm, and for a submerged log $h_{dc,m} = 4.1 \pm 0.8$ mm (see Text S2, Figure S1, and Table S2 in Supporting Information S1). Combining both tests, the declogging occurred over a depth of ≈ 2.4 times d_m.

Finally, the clogging test (C1 in Table 1) studied if log placements could inhibit clogging. The logs were placed on a clean bed, the discharge was set, and the walnut grit slurry was added and then circulated for 2 hr. Top view images were taken in the drained flume before and after adding the walnut grit.

2.2. Surface Declogging

The degree of surface declogging, $\Delta\xi$, was defined as the reduction in surface area clogged by fine sediment normalized by the original clogged area. A digital camera and two light sources were mounted on a movable traverse. Fifteen high-resolution images (0.18 mm/pixel) were taken, covering the entire test section with a minimum overlap of 5 cm between images. Within each 4 cm × 4 cm region of interest (ROI), A_c was defined as the fraction of area covered with fine sediment, called the clogged fraction. The number of ROIs varied between tests (14–36) and were co-located with velocity measurements.

The clogged fraction was estimated using the image processing software Image J (Schindelin et al., 2012). The minimum detectable area was set to 1 mm^2, which averaged over individual grains of both sizes. The workflow for test D1 and two selected ROIs is illustrated in Figures 1c–1p. The original images (Figures 1e, 1h, 1k, and 1n) were converted to grayscale (Figures 1f, 1i, 1l, 1o). ROIs with a low presence of fines, defined by gray pixel values > 100 in the image histogram were analyzed with the Yen method (Figures 1j and 1p; Yen et al. (1995)). The Shanbhag method was used on ROIs with a high presence of fines (gray <100, Figures 1g and 1m; see Text S3 and Figure S2 in Supporting Information S1; Shanbhag (1994)). The fractional clogged areas before $A_{c,pre}$ and after $A_{c,post}$ each test were used to define the degree of surface declogging, $\Delta\xi$. To remove outliers, the standard deviation (σ) of $A_{c,pre}$ was used as a threshold value. Specifically, if $A_{c,pre} - A_{c,post} < \sigma_{Ac,pre}$, then we set $\Delta\xi = 0$, otherwise
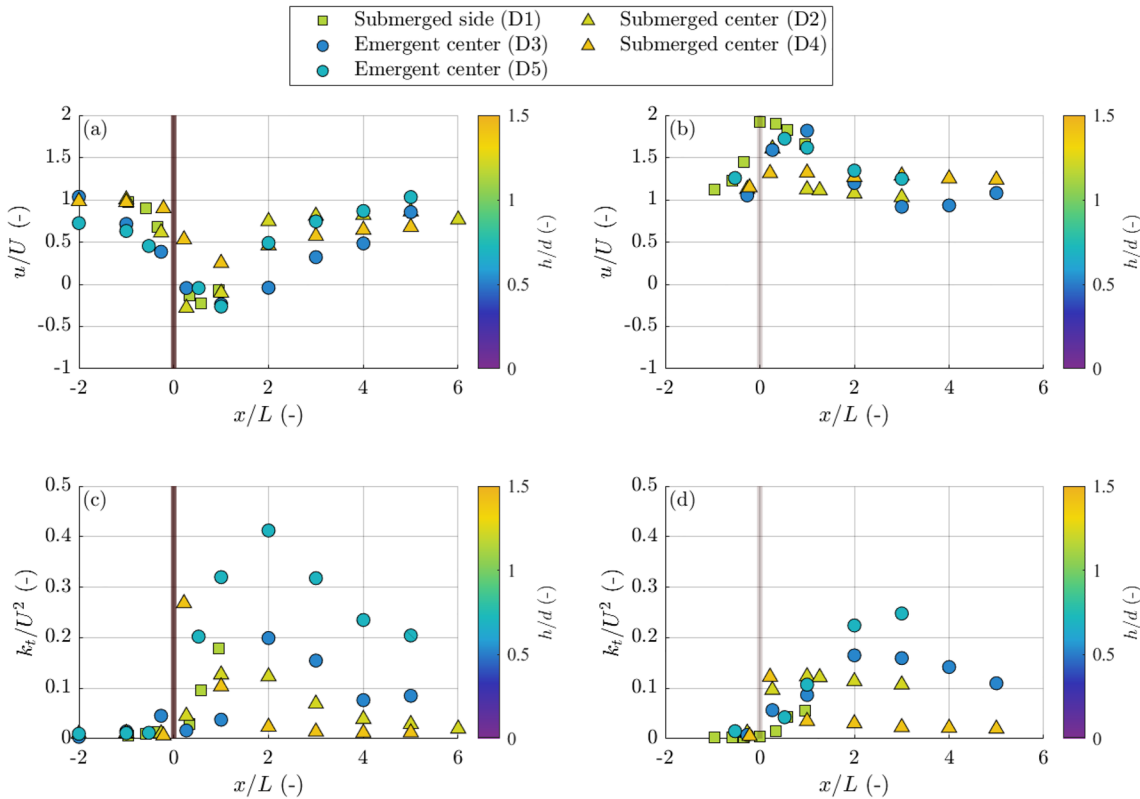
$$\Delta\xi = \frac{A_{c,pre} - A_{c,post}}{A_{c,pre}} \tag{2}$$

3. Results and Discussion

3.1. Flow Structures

Longitudinal profiles of velocity and TKE were measured at the log center (Figures 2a and 2c) and adjacent to the log (Figures 2b and 2d). Directly downstream of the log, the time-mean velocity in the wake was reduced

Figure 2. Longitudinal profiles of normalized time-mean velocity u and turbulent kinetic energy k_t along the log center (a, c) and adjacent to the log (b, d) for tests D1-D5 with different submergence levels h/d.

compared to the upstream, $u/U < 1$ (Figure 2a), and in most cases negative velocity was measured, indicating the presence of a recirculation zone. The velocity adjacent to the log was accelerated, reaching an average of $u/U = 1.7$ for all tests (Figure 2b).

The normalized TKE, k_t/U^2, was elevated downstream of the log (Figure 2c). Consistent with previous studies (Schalko et al., 2021), TKE was higher for emergent (circles) compared to submerged (square and triangle) logs. On average, peak k_t/U^2 was 0.31 for emergent center logs, but only 0.20 for submerged center logs. The location of the peak TKE shifted downstream as the submergence level h/d decreased (Figure 2c). For example, in test D4 with $h/d = 1.40$, the peak TKE was located at $x/L = 0.21$, while in test D3 with $h/d = 0.53$, the peak TKE was located at $x/L = 2$. Adjacent to the log, turbulence elevation was not as pronounced as in the wake (Figure 2d), but was still elevated compared to the upstream region.

3.2. Surface Declogging

Figure 3 presents the position of measurement and degree of surface declogging, $\Delta \xi$, for declogging tests D1-D5. Yellow and green symbols denote ROIs with greater than 50% surface declogging. Emergent logs were more effective in declogging the surface than submerged logs. In particular, test D5 (Figure 3e) exhibited the largest footprint of declogging (most yellow and green points), which extended over the wake width and from $x/L = 0$ to 3. The submerged logs (tests D1, D2, D4; Figures 3a, 3b, and 3d) produced some regions with strong declogging (yellow points), but with a less extensive spatial footprint than the emergent logs. Declogging increased with increasing log size, for example, $\Delta \xi = 66 \pm 7$ for test D2 compared to $\Delta \xi = 32 \pm 5$ for test D4 (Table 1; Figures 3b and 3d). The regions of elevated declogging aligned with areas of heightened velocity adjacent to the log (Figure 2b) and elevated turbulence in the wake region downstream of the log (Figure 2c). For example, in test D1 (Figure 3a) a submerged side log produced declogging adjacent to the log coincident with regions of increased velocity, but not significantly increased TKE (squares in Figures 2b and 2d). In contrast, for test D5 (Figure 3e) an emergent center log produced elevated declogging along the centerline of the wake, where velocity was diminished, but TKE was elevated (circles, Figures 2a and 2c).
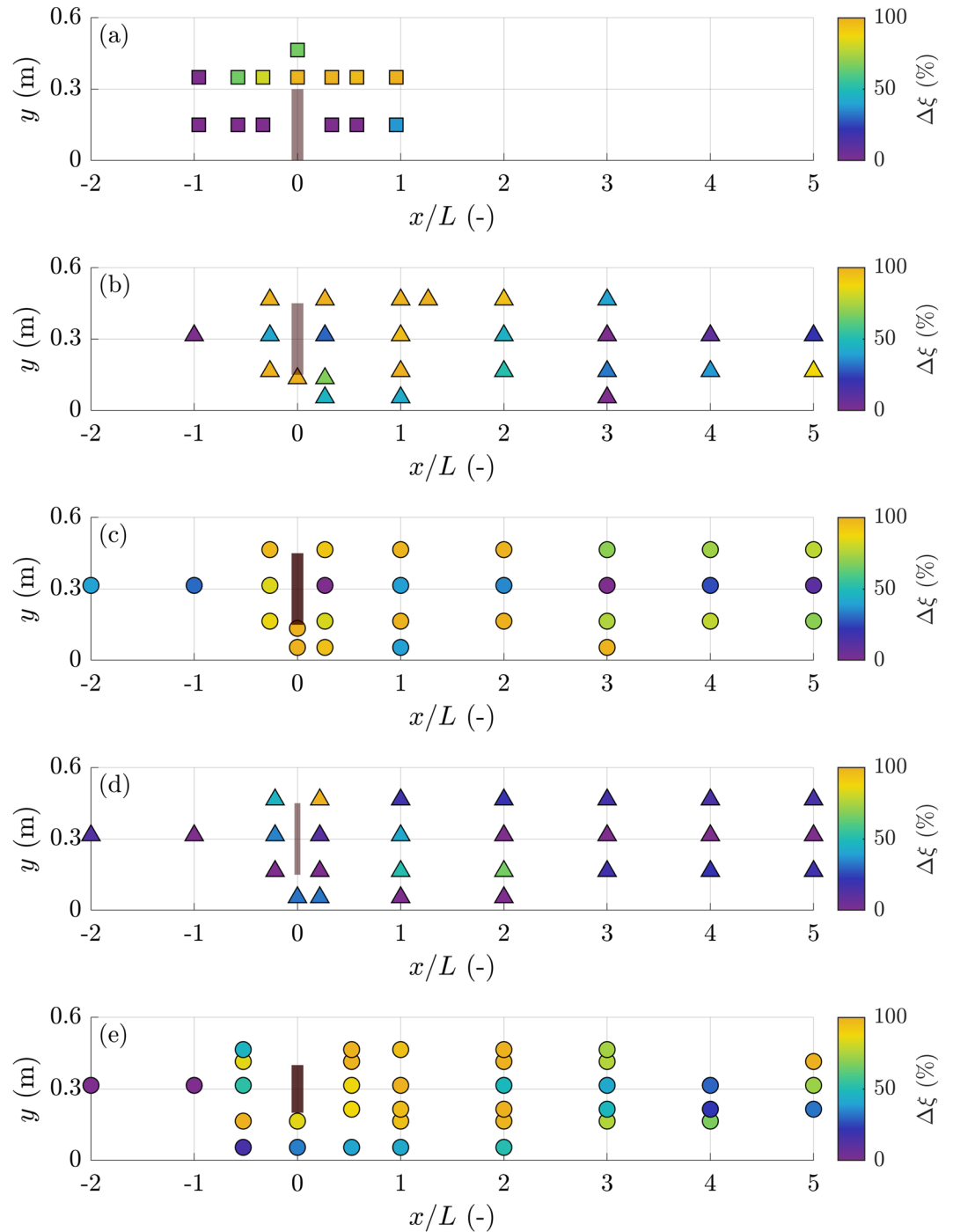
Figure 3. Aerial sketch of tests D1-D5 (a)–(e) with symbols indicating declogging measurement locations. Symbol colors show degree of declogging $\Delta\xi$. Purple symbols show ROIs that resulted in zero declogging by applying Equation 2. Emergent logs are colored in dark brown and submerged logs in light brown. Squares correspond to side placement, triangles to submerged and circles to emergent logs. Flow direction from left to right.

Noting that declogging occurred both in regions of elevated velocity and TKE, both flow parameters were considered to define a threshold for surface declogging. We defined a non-dimensional instantaneous bed-shear stress θ that incorporated both the time-mean u and turbulent velocity $\sqrt{k_t}$ (e.g., Tinoco & Coco, 2016).

$$\theta = \frac{C_f\left(u^2 + \beta k_t\right)}{(s-1)gd_m} \tag{3}$$
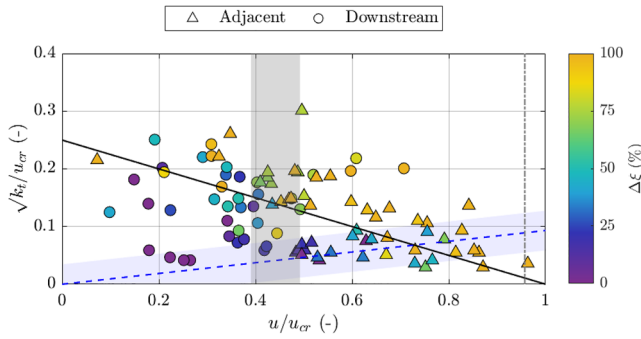
Figure 4. Square root of turbulent kinetic energy $\sqrt{k_t}$ versus time-mean flow velocity u normalized with critical velocity u_{cr} at locations of declogging measurements with circles located downstream and triangles adjacent to log (Figure 1). 13 out of 103 data points exhibited zero declogging based on Equation 2. Equation 5 is plotted as a solid black line. Dashed blue line shows bed-generated turbulence including a blue shaded area denoting standard error of measured velocities. Gray shaded area is range of tested U/u_{cr}. Dashed-dotted gray line depicts normalized critical velocity for gravel motion based on Schalko and Nepf (2020).

in which, C_f is the bed friction coefficient that can be determined by applying the semi-empirical equation in Julien (2010), s is relative sediment density, g is gravitational acceleration, d_m is mean grain size, and β is a scaling factor describing the different efficiency with which time-mean versus instantaneous turbulent non-dimensional bed-shear stress acts on the bed. Next, we defined a non-dimensional critical bed-shear stress θ_{cr} above which declogging is initiated. In the absence of turbulence ($k_t = 0$), this non-dimensional critical bed-shear stress θ_{cr} defines a critical velocity u_{cr}:

$$\theta_{cr} = \frac{C_f u_{cr}^2}{(s-1)g d_m} \tag{4}$$

Note that Equation 4 defines the process of declogging associated with transport and/or erosion of the gravel. By equating Equation 3 with Equation 4, we defined the boundary ($\theta = \theta_{cr}$) above which declogging can occur within $\left(\sqrt{k_t}, u\right)$ parameter space. Normalizing by the critical velocity, we obtain:

$$\frac{\sqrt{k_t}}{u_{cr}} = \frac{1}{\beta} - \frac{1}{\beta}\frac{u}{u_{cr}} \tag{5}$$

The scaling factor β was found by fitting the measurements of tests D1-D5 to Equation 5, as shown in Figure 4. The measurements of strong declogging (>50%, green to yellow points) predominantly fell above the boundary, whereas measurements of weak to negligible declogging (<50%, blue to purple points) fell below it. The boundary shown in Figure 4 has a slope of $m = \beta^{-1} = 0.25$, suggesting that $\beta = 4.0 \pm 0.4$, yielding $u_{cr} = 0.48 \pm 0.02$ m/s. Note that the uncertainty associated with β and u_{cr} correspond to standard errors based on variation of slope and intercept. The value of u_{cr} is comparable to the threshold for gravel motion of $u_{cr,ref} = 0.46$ m/s ($u_{cr,ref}/u_{cr} = 0.96$) with $\theta_{cr} = 0.047$ based on a previous study using the same gravel (Schalko & Nepf, 2020), plotted as a vertical gray dash-dot line in Figure 4. Given that u_{cr} was consistent with the critical velocity to initiate motion of the gravel bed ($u_{cr,ref}$), it seems likely that Equation 5 can be applied to beds of other gravel size by appropriately adjusting the critical velocity, for example, based on $u_{cr} = \frac{u_*}{\sqrt{C_f}}$ with shear velocity u_* and the Shields diagram.

The bed-generated turbulence ($\sqrt{k_t}/u$) is shown with a dashed blue line in Figure 4, based on the average velocity over the bare gravel for all tests at the beginning of the test section. The many points falling above this line highlight the contribution of the logs to channel turbulence. The gray shaded area illustrates the tested normalized channel-averaged flow velocities in this study. Adjacent to a log (triangles), declogging was predominantly associated with velocity exceeding the channel-averaged velocity (gray shaded area). In contrast, downstream of the log (circles), declogging was observed in regions of velocity below the threshold for gravel motion, but with elevated turbulence. As velocity approached zero, declogging occurred when the turbulent velocity reached about ten-times the settling velocity of the fines ($\sqrt{k_t} = 13.3\, w_s$).

Finally, test C1 was designed to examine the potential for log placements to prevent clogging. Logs were placed on an initially clean gravel bed (Figure S3a in Supporting Information S1) and the channel was exposed to 2 hr of walnut grit transport. The resulting surface clogging is shown in Figure S3b in Supporting Information S1. After the test, regions showing clean gravel (white) were located adjacent to the log and in the log wake, similar to the findings of tests D1-D5. That is, clogging was prevented from occurring in the same regions previously observed to produce declogging of a pre-clogged bed. With regard to test C1, larger logs (larger d or L; Log 2 in Figure 1) had a stronger effect to reduce or inhibit surface clogging compared to smaller logs (Log 5 in Figure 1). Compared to the total area of the logs (0.11 m²), approximately 0.14 m² were protected from clogging, corresponding to 1.3 times the footprint of all logs. The ratio varied with submergence. Specifically, for emergent logs, 1.9 times the log's footprint was protected from clogging, while this factor was reduced to 0.7 for submerged logs.

Our results suggest that declogging occurs locally and transported fines may deposit further downstream. The focus of this study was on ordinary flow conditions. During higher flow conditions, larger wood placements such as logjams may elevate the flood risk leading to backwater rise (Ruiz-Villanueva et al., 2018). Note that with increasing backwater rise the pressure gradient upstream of logjams is also increasing, leading to elevated

hyporheic exchange flow, which benefits declogging (Ader et al., 2021; Doughty et al., 2020; Sawyer et al., 2011). This trade-off should be accounted for during the design of wood placements.

4. Conclusions

This study showcased the potential of deliberate wood placements to locally reduce fine sediment accumulation (clogging) by modifying local flow conditions. This has positive benefits for river ecology. Both elevated turbulence in the log wake and elevated velocity adjacent to the log were found to trigger declogging, and these flow parameters were combined to describe a threshold for declogging. The critical velocity for declogging was found to be comparable to the threshold velocity for gravel motion, which facilitates the application of the findings to beds of different gravel size. For regions where velocity approached zero, turbulent velocities exceeding 10 times the settling velocity of the fines were required for declogging. Emergent logs produced a larger footprint of declogging, relative to log dimension, due to their stronger influence on the mean and turbulent flow. Similarly, the area of bed protected from clogging was also proportional to the log footprint, but larger for emergent compared to submerged logs.

Data Availability Statement

The data set for this study is available in Schalko et al. (2023) (CC BY 4.0). Post-processing codes of Nortek Vectrino raw data are available at https://tkeanalyst.readthedocs.io/. Flow data (Q, h) listed in Table S1 (Supporting Information S1) was retrieved from http://www.hydrodaten.admin.ch/ and river width B was measured using https://map.geo.admin.ch.

References

Ader, E., Wohl, E., McFadden, S., & Singha, K. (2021). Logjams as a driver of transient storage in a mountain stream. *Earth Surface Processes and Landforms*, *46*(3), 701–711. https://doi.org/10.1002/esp.5057

Cunningham, A. B., Anderson, C. J., & Bouwer, H. (1987). Effects of sediment-laden flow on channel bed clogging. *Journal of Irrigation and Drainage Engineering*, *113*(1), 106–118. https://doi.org/10.1061/(asce)0733-9437(1987)113:1(106)

Doughty, M., Sawyer, A. H., Wohl, E., & Singha, K. (2020). Mapping increases in hyporheic exchange from channel-spanning logjams. *Journal of Hydrology*, *587*, 124931. https://doi.org/10.1016/j.jhydrol.2020.124931

Dubuis, R., & De Cesare, G. (2023). The clogging of riverbeds: A review of the physical processes. *Earth-Science Reviews*, *239*, 104374. https://doi.org/10.1016/j.earscirev.2023.104374

Einstein, H. A. (1968). Deposition of suspended particles in a gravel bed. *Journal of the Hydraulics Division*, *94*(5), 1197–1206. https://doi.org/10.1061/jyceaj.0001868

Faustini, J. M., & Jones, J. A. (2003). Influence of large woody debris on channel morphology and dynamics in steep, boulder-rich mountain streams, western Cascades, Oregon. *Geomorphology*, *51*(1–3), 187–205. https://doi.org/10.1016/S0169-555X(02)00336-7

Gippel, C. J. (1995). Environmental hydraulics of large woody debris in streams and rivers. *Journal of Environmental Engineering*, *121*(5), 388–395. https://doi.org/10.1061/(ASCE)0733-9372(1995)121:5(388)

Goring, D. G., & Nikora, V. I. (2002). Despiking acoustic doppler velocimeter data. *Journal of Hydraulic Engineering*, *128*(1), 117–126. https://doi.org/10.1061/(ASCE)0733-9429(2002)128:1(117)

Gurnell, A. M., PiéGay, H., Swanson, F. J., & Gregory, S. V. (2002). Large wood and fluvial processes: Large wood and fluvial processes. *Freshwater Biology*, *47*(4), 601–619. https://doi.org/10.1046/j.1365-2427.2002.00916.x

Jones, J. I., Murphy, J. F., Collins, A. L., Sear, D. A., Naden, P. S., & Armitage, P. D. (2012). The impact of fine sediment on macro-invertebrates. *River Research and Applications*, *28*(8), 1055–1071. https://doi.org/10.1002/rra.1516

Julien, P. Y. (2010). *Erosion and sedimentation* (2nd ed.). Cambridge University Press.

Keller, E. A., & Swanson, F. J. (1979). Effects of large organic material on channel form and fluvial processes. *Earth Surface Processes*, *4*(4), 361–380. https://doi.org/10.1002/esp.3290040406

Kemp, P., Sear, D., Collins, A., Naden, P., & Jones, I. (2011). The impacts of fine sediment on riverine fish. *Hydrological Processes*, *25*(11), 1800–1821. https://doi.org/10.1002/hyp.7940

Kondolf, G. M., Gao, Y., Annandale, G. W., Morris, G. L., Jiang, E., Zhang, J., et al. (2014). Sustainable sediment management in reservoirs and regulated rivers: Experiences from five continents. *Earth's Future*, *2*(5), 256–280. https://doi.org/10.1002/2013ef000184

Lisle, T. E. (1989). Sediment transport and resulting deposition in spawning gravels, north coastal California. *Water Resources Research*, *25*(6), 1303–1319. https://doi.org/10.1029/wr025i006p01303

Müller, S., Follett, E. M., Ouro, P., & Wilson, C. (2022). Influence of channel-spanning engineered logjam structures on channel hydrodynamics. *Water Resources Research*, *58*(12), e2022WR032111. https://doi.org/10.1029/2022wr032111

Owens, P. N., Batalla, R. J., Collins, A. J., Gomez, B., Hicks, D. M., Horowitz, A. J., et al. (2005). Fine-grained sediment in river systems: Environmental significance and management issues. *River Research and Applications*, *21*(7), 693–717. https://doi.org/10.1002/rra.878

Roni, P., Beechie, T., Pess, G., & Hanson, K. (2015). Wood placement in river restoration: Fact, fiction, and future direction. *Canadian Journal of Fisheries and Aquatic Sciences*, *72*(3), 466–478. https://doi.org/10.1139/cjfas-2014-0344

Ruiz-Villanueva, V., Badoux, A., Rickenmann, D., Böckli, M., Schläfli, S., Steeb, N., et al. (2018). Impacts of a large flood along a mountain river basin: Unravelling the geomorphic response and large wood budget in the upper Emme River (Switzerland). *Earth Surface Dynamics Discussions*, 1–42. https://doi.org/10.5194/esurf-2018-44

Sawyer, A. H., Bayani Cardenas, M., & Buttles, J. (2011). Hyporheic exchange due to channel-spanning logs. *Water Resources Research*, *47*(8). https://doi.org/10.1029/2011WR010484

Schälchli, U. (1992). The clogging of coarse gravel river beds by fine sediment. *Hydrobiologia*, *235*(1), 189–197. https://doi.org/10.1007/bf00026211

Schalko, I., & Nepf, H. (2020). How to design wood accumulation patches to increase flow variability and deposition—A flume study. In *Proceedings of the 10th Conference on Fluvial Hydraulics. Delft, The Netherlands*. CRC Press. Retrieved from https://www.taylorfrancis.com/books/9781000294361

Schalko, I., Ponce, M., Lassar, S., Schwindt, S., Haun, S., & Nepf, H. (2023). Dataset: Flow and turbulence due to wood contribute to declogging of gravel bed [Dataset]. Zenodo. https://doi.org/10.5281/ZENODO.10419521

Schalko, I., Wohl, E., & Nepf, H. M. (2021). Flow and wake characteristics associated with large wood to inform river restoration. *Scientific Reports*, *11*(1), 8644. https://doi.org/10.1038/s41598-021-87892-7

Schindelin, J., Arganda-Carreras, I., Frise, E., Kaynig, V., Longair, M., Pietzsch, T., et al. (2012). Fiji: An open-source platform for biological-image analysis. *Nature Methods*, *9*(7), 676–682. https://doi.org/10.1038/nmeth.2019

Schnauder, I., Anlanger, C., & Koll, K. (2022). Wake flow patterns and turbulence around naturally deposited and installed trees in a gravel bed river. *International Review of Hydrobiology*, *107*(1–2), 22–33. https://doi.org/10.1002/iroh.202102096

Schwindt, S., Negreiros, B., Ponce, M., Schalko, I., Lassar, S., Barros, R., & Haun, S. (2023). Fuzzy-logic indicators for riverbed de-clogging suggest ecological benefits of large wood. *Ecological Indicators*, *155*, 111045. https://doi.org/10.1016/j.ecolind.2023.111045

Sear, D. A. (1993). Fine sediment infiltration into gravel spawning beds within a regulated river experiencing floods: Ecological implications for salmonids. *Regulated Rivers: Research and Management*, *8*(4), 373–390. https://doi.org/10.1002/rrr.3450080407

Shanbhag, A. G. (1994). Utilization of information measure as a means of image thresholding. *CVGIP: Graphical Models and Image Processing*, *56*(5), 414–419. https://doi.org/10.1006/cgip.1994.1037

Tinoco, R. O., & Coco, G. (2016). A laboratory study on sediment resuspension within arrays of rigid cylinders. *Advances in Water Resources*, *92*, 1–9. https://doi.org/10.1016/j.advwatres.2016.04.003

Wilhelmsen, K., Sawyer, A. H., Marshall, A., McFadden, S., Singha, K., & Wohl, E. (2021). Laboratory flume and numerical modeling experiments show log jams and branching channels increase hyporheic exchange. *Water Resources Research*, *57*(9), e2021WR030299. https://doi.org/10.1029/2021wr030299

Wohl, E., Bledsoe, B. P., Jacobson, R. B., Poff, N. L., Rathburn, S. L., Walters, D. M., & Wilcox, A. C. (2015). The natural sediment regime in rivers: Broadening the foundation for ecosystem management. *BioScience*, *65*(4), 358–371. https://doi.org/10.1093/biosci/biv002

Wohl, E., Kramer, N., Ruiz-Villanueva, V., Scott, D. N., Comiti, F., Gurnell, A. M., et al. (2019). The natural wood regime in rivers. *BioScience*, *69*(4), 259–273. https://doi.org/10.1093/biosci/biz013

Wohl, E., & Scott, D. N. (2017). Wood and sediment storage and dynamics in river corridors: Wood and sediment dynamics in river corridors. *Earth Surface Processes and Landforms*, *42*(1), 5–23. https://doi.org/10.1002/esp.3909

Wood, P. J., & Armitage, P. D. (1997). Biological effects of fine sediment in the lotic environment. *Environmental Management*, *21*(2), 203–217. https://doi.org/10.1007/s002679900019

Wooster, J. K., Dusterhoff, S. R., Cui, Y., Sklar, L. S., Dietrich, W. E., & Malko, M. (2008). Sediment supply and relative size distribution effects on fine sediment infiltration into immobile gravels. *Water Resources Research*, *44*(3). https://doi.org/10.1029/2006wr005815

Yen, J.-C., Chang, F.-J., & Chang, S. (1995). A new criterion for automatic multilevel thresholding. *IEEE Transactions on Image Processing*, *4*(3), 370–378. https://doi.org/10.1109/83.366472